RADIATION RESEARCH **185**, 182–189 (2016)
0033-7587/16 $15.00

DOI: 10.1667/RR14190.1

Mast Cells Contribute to Radiation-Induced Vascular Hyperpermeability

Kyung Ran Park,[a,1] Wayne L. Monsky,[a,2] Chang Geol Lee,[a,3] Chang Ho Song,[b] Dong Heui Kim,[c] Rakesh K. Jain[a] and Dai Fukumura[a,4]

[a] *Edwin L. Steele Laboratory, Department of Radiation Oncology, Massachusetts General Hospital, Harvard Medical School, Boston, Massachusetts;* [b] *Department of Anatomy, Chonbuk National University Medical School, Chonju, Republic of Korea; and* [c] *Department of Basic Science, Institute of Basic Medical Science, Yonsei University Wonju College of Medicine, Wonju, Republic of Korea*

Park, K. R., Monsky, W. L., Lee, C. G., Song, C. H., Kim, D. H., Jain, R. K. and Fukumura, D. Mast Cells Contribute to Radiation-Induced Vascular Hyperpermeability. *Radiat. Res.* 185, 182–189 (2016).

Induction of vascular hyperpermeability is one of the early vascular responses to radiation exposure and is considered to contribute to subsequent fibrosis and tissue injuries. However, the mechanism underlying radiation-induced hyperpermeability has not yet been clearly elucidated. Here, we provide experimental evidence indicating that mast cells contribute to the increase in vascular permeability for albumin in normal mouse skin after irradiation. Vascular permeability in the skin of C3H mice increased after 2, 15 and 50 Gy irradiation, peaked at 24 h after irradiation and gradually decreased thereafter to the baseline level within 3–10 days. Both the extent and duration of hyperpermeability were dose dependent. We found significant degranulation of mast cells in the skin after 15 Gy irradiation. To further investigate the role of mast cells in the radiation-induced increase in vascular permeability, we measured vascular permeability in the skin of mast cell-deficient mice (WW^v) and their wild-type littermates at 24 h after irradiation. Vascular permeability in WW^v mice did not change, whereas that in wild-type mice significantly increased after irradiation. There were no appreciable changes in the total tissue levels of vascular endothelial growth factor or endothelial nitric oxide synthase after 15 Gy irradiation and there was no detectable expression of inducible nitric oxide synthase. Collectively, these results show that exposure to radiation induces vascular hyperpermeability in a dose-dependent manner and that mast cells contribute to this process.

INTRODUCTION

The vascular endothelium separates the blood from tissues and regulates the exchange of materials between these compartments. It has been postulated that radiation damages the integrity of the microvascular endothelium, thereby inducing transvascular hyperpermeability to plasma proteins, with subsequent fibrin deposition in the extravascular spaces. The newly deposited fibrin is eventually replaced by collagen fibers, resulting in fibrosis and parenchymal cell atrophy, which are characteristic of the late phase of radiation-induced injuries in normal tissues (*1–3*).

Numerous studies have demonstrated an increase in macromolecular extravasation after irradiation in various normal tissues (*1–16*), as well as in tumors (*17*). These previous studies have mostly determined the total amount of extravasated macromolecules that result from an increase in the permeability surface area product (defined by the vascular permeability and vascular surface area); however, vascular permeability itself has not yet been measured directly.

We previously reported a novel method to measure the average effective permeability of microvessels in three-dimensional tissues, which facilitated direct measurements of the average vascular permeability itself using intravital quantitative fluorescence microscopy (*18–20*). In brief, a fluorescent-labeled molecule is injected into the circulation and then monitored as it extravasates at a particular site of the surface area of skin. This approach facilitates explicit consideration of the three-dimensional transport of molecules within the observed tissue. Furthermore, the light-collecting characteristics of the optical system can be used to determine how the detected fluorescence intensity is related to the extravasation of fluorescent molecules. By measuring vessel geometry and the fluorescence intensity distribution at various time points, the permeability surface area product per unit volume, fractional vascular volume and average effective vascular permeability could also be calculated. Therefore, in the current study, we applied this technique to measure changes in vascular permeability in mouse skin after irradiation.

[1] Current address: Department of Radiation Oncology, Ewha Womans University Medical Center, Seoul, Republic of Korea.
[2] Current address: Department of Radiology, University of Washington Medical Center, Seattle, WA 98195.
[3] Current address: Department of Radiation Oncology, Yonsei University College of Medicine, Seoul, Republic of Korea.
[4] Address for correspondence: Department of Radiation Oncology, Massachusetts General Hospital, 100 Blossom Street, COX-7, Boston, MA 02114; e-mail: dai@steele.mgh.harvard.edu.

One reasonable mechanism to account for the early increase in vascular permeability after irradiation is degranulation of the mast cells (*21*). Multiple cytokines with the ability to increase vascular permeability [e.g., histamine, serotonin, vascular endothelial growth factor (VEGF)] are normally stored in tissue mast cells (*22*) and therefore, are released by mast cell degranulation (*23*). Among these various agents, histamine has been reported to be the most important cytokine released from the mast cells with respect to the observed induction in vascular permeability after irradiation (*16, 24–29*). Albrecht *et al.* reported mast cell degranulation in *ex vivo* skin culture models at 2 h after 5 Gy irradiation (*30*). Other studies have shown that treatment of an antihistamine and mast cell stabilizer reduced the increase of vascular permeability after irradiation (*10, 16, 29, 31*). To directly test the hypothesis, we measured the average permeability of microvessels and performed mast cell degranulation analysis after irradiation.We also determined the expression of other known regulators of vascular permeability, including VEGF and endothelial nitric oxide synthase (eNOS). VEGF, also known as vascular permeability factor, is a multifunctional cytokine with an important role in the regulation of physiological and pathological angiogenesis (*32*). VEGF is one of the most potent vascular permeabilizing agents with potency 50,000 times greater than that of histamine. Upregulation of VEGF is associated with radiation-induced blood-spinal cord barrier breakdown (*33*). Nitric oxide (NO) is known to regulate microvascular permeability (*34*). In particular, eNOS is a key mediator of VEGF-induced vascular permeability (*35*).

In the current study, we analyzed: 1. The vascular permeability in normal mouse skin before and at various time points after exposure to different single doses of local irradiation; 2. The contribution of mast cells to radiation-induced vascular hyperpermeability; and 3. Expression of VEGF and NOSs in the skin after irradiation.

MATERIALS AND METHODS

Animals and Experimental Protocol

C3H mice that are bred and maintained in our gnotobiotic colony were used in these experiments. Dorsal chambers were implanted in the C3H mice for intravital microscopy as described previously (*19*). Vascular permeability in the dorsal chambers was determined before irradiation for the baseline value and then at 1, 3, 5 and 24 h and at 3, 5 and 10 days after irradiation. To discern the role of mast cells in the radiation-induced increase of vascular permeability, we also determined the effect of 15 Gy irradiation on the vascular permeability in the skin of mast cell-deficient WBB6F1/J-Kit^{W}/Kit^{W-v} (WW^{v}) mice and their wild-type littermates (Jackson Laboratory, Bar Harbor, ME). All animal studies were approved by Institutional Animal Care and Use Committee of Massachusetts General Hospital (Boston, MA).

Radiation Protocol

Single radiation doses of 2, 15 and 50 Gy were administered to the dorsal chamber in the mice with a cesium-137 irradiator at a dose rate of 5.7 Gy/min, and vascular permeability was measured. A single dose of 15 Gy was delivered to the hind leg of C3H mice with a cesium-137 irradiator, and Northern and Western blot analyses were performed to determine the expression levels of *VEGF* mRNA, as well as VEGF, eNOS and inducible NOS (iNOS) protein. A single 15 Gy dose was delivered to the left ear of WW^{v} and wild-type mice to evaluate the radiation-induced changes in vascular permeability. Western blot analysis was also performed to determine the radiation-induced effects on the protein expression of VEGF, eNOS and iNOS. The radiation-induced changes in mast cells were assessed with Giemsa staining and electron microscopic examination.

Measurement of Vascular Permeability

Tracers. Fluorescent isothiocyanate (FITC)-labeled dextran (2,000,000 M$_r$; Sigma-Aldrich, St. Louis, MO) was used for vessel localization and measurements of vascular surface area. Albumin labeled with either cyanine-5 (Amersham™ Life Science, Arlington Heights, IL) or tetramethylrhodamine (Molecular Probes®, Eugene, OR) was used for measuring permeability.

Intravital microscopy. For contrast enhancement of the intravascular space of the small blood vessels, a bolus of 0.1 ml of FITC-dextran (150,000 M$_r$; 5 mg/100 μl of 0.9% NaCl; Sigma-Aldrich) was injected into the tail vein of the mice 5 min prior to the recordings.

Microcirculatory parameters of normal mouse skin in the dorsal chambers were evaluated with an intravital microscope (Axioplan; Carl Zeiss Microscopy, Oberkochen, Germany) equipped with filter sets for rhodamine (excitation peak at 541 nm, emission peak at 572 nm), cyanine-5 (excitation peak at 649 nm, emission peak at 670 nm) and FITC (excitation peak at 450–490 nm, emission peak at 515–545 nm); an intensified CCD video camera (C2400-88; Hamamatsu Photonics K.K., Hamamatsu, Japan); photomultiplier tube (9203B; EMI, Rockaway, NJ); super VHS video recorder (SVO-9500 MD; Sony, Tokyo, Japan); and thermal video printer (P67U; Mitsubishi, Somerset, NJ). In all experiments, transillumination or epi-illumination (100W mercury lamp, model 770; Opti-Quip Inc., Highland Mills, NY) was used to locate and stereotactically record the vessel region of interest using video photo documentation to enable relocalization after irradiation. To minimize the variation in microvascular parameters, the same vessels were observed for each experiment before and after irradiation (Fig. 1A and B). For each experiment, the relative change from the pretreatment baseline is reported. To facilitate relocalization of the vessels after each radiation treatment, the images of the target vessels were recorded at 2.5×, 5×, 10× and 20× objectives using a thermal video printer (P67U; Mitsubishi, Somerset, NJ), and marker coordinates were recorded at each magnification.

Microscopic measurements. Intravital microscopic measurement of vascular permeability was performed in the dorsal skin chamber for each mouse (*19*). Permeability to albumin labeled with either cyanine-5 or rhodamine was determined at an initial time before irradiation and again at the same, stereotactically located vessels with the alternate color-labeled albumin at 1, 3, 5 and 24 h and 3, 5 and 10 days after irradiation. All vessels analyzed were well perfused throughout the measurements.

Permeability calculations. Albumin vascular permeability was determined as described previously (*20, 36*). After bolus injection of fluorescently labeled bovine serum albumin (BSA), fluorescence intensity was measured for 10 s per observation at 2 min intervals for 21 min. The P value was calculated as $P = (1 - HT) \times V/S \{1/(I_0 - I_b) \times dI/dt + 1/K\}$, where I is the average fluorescence intensity of the whole image, I_0 (the background intensity) is the value of I immediately after all the vessels become filled with the fluorescent-labeled BSA, HT is the average hematocrit level in the vessels, V and S are the total volume and total surface area of the vessels captured by the microscope, respectively, and K is the time constant for the plasma clearance of BSA.

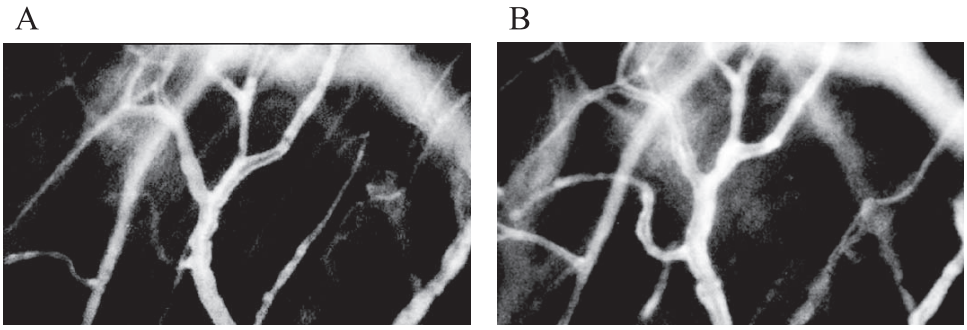

FIG. 1. Fluorescent image of C3H mouse skin as recorded during intravital microscopic examination before irradiation (panel A) and at one day after 50 Gy irradiation (panel B). The same vessels were observed for each experiment before and after irradiation. The total volume and total surface area of the vessels were measured using the fluorescent image.

Mast Cell Degranulation Analysis: Giemsa Staining

Samples of irradiated and nonirradiated mouse ear skin were obtained after sacrificing the mice and were processed for 1 μm Epon-embedded, Giemsa-stained sections (*37, 38*). The sections were examined by an observer blinded to the identity of the individual specimens. The number of dermal mast cells per mm^2 of dermis was determined (at 1,000× magnification), and the cells were classified as: extensively degranulated (>50% of cytoplasmic granules exhibited fusion, staining alterations and extrusion from the cells); slightly to moderately degranulated (10–50% of the granules exhibited fusion of discharge); or normal (*39, 40*).

Mast Cell Degranulation Analysis: Electron Microscopy

Samples of the mouse ear skin were shaved and cut into small pieces. The tissue pieces were immediately fixed with 2.5% glutaraldehyde in 0.1 *M* phosphate buffer (pH 7.4) at 4°C for 2 h and post-fixed with 2% OsO_4 in the same buffer at 4°C for 90 min. The tissues were then washed with 0.1 *M* phosphate buffer, dehydrated in graded ethanol and embedded in Epon epoxy resin. Ultrathin sections were stained with uranyl acetate and lead citrate, and then observed under a transmission electron microscope (JEM-1200 EXII; JEOL Ltd., Tokyo, Japan) at an 80 kV accelerating voltage.

Western Blot Analysis

The skin tissue samples were homogenized in a lysis buffer (0.1 *M* NaCl, 0.01 *M* Tris-HCl, pH 7.5, 1 *M* EDTA and 1 μg/ml aprotinin). The homogenates were centrifuged at 7,000*g* for 15 min at 4°C, and the supernatants were used as protein samples. The protein concentration of the supernatants was subsequently determined by comparison with a known concentration of BSA with the Micro BCA Protein Assay Kit (Pierce™ Biotechnology/Thermo Fisher Scientific Inc., Rockford, IL). Sodium dodecyl sulfate (SDS) gel electrophoresis was performed in a 10% polyacrylamide gel under nonreducing conditions. Lysates equivalent to 40 μg of protein from each sample were run on the gel for 90 min at 20 mA, together with a size marker (rainbow-colored protein; Amersham Life Science Inc., Cleveland, OH). The electrophoresis running buffer contained 25 m*M* Tris base, 250 m*M* glycine and 0.1% SDS. The proteins on the gel were subsequently transferred to a polyvinylidene fluoride transfer membrane (Micron Separations Inc., Westborough, MA) in a buffer containing 20% methanol, 39 m*M* glycine, 48 m*M* Tris base and 0.4% SDS.

Northern Blot Analysis

Mouse skin from the left hind leg (100 mg) was removed and placed in 1 ml of TRIzol® RNA isolation reagent (Gibco®, Grand Island, NY) at room temperature and homogenized for 15 s with a Polytron™ homogenizer (Brinkmann™/Kinematica Inc., Bohemia, NY). The homogenate was then mixed with 0.2 ml of chloroform and centrifuged for 15 min at 12,000*g* at 4°C. The aqueous phase was transferred to a fresh tube, and the total RNA was extracted. Total RNA was separated by electrophoresis on a 1% agarose gel containing 1.7% (vol/vol) formaldehyde. RNA (30 μm) was transferred to a GeneScreen Plus® membrane (PerkinElmer® Inc., Waltham, MA), and hybridized with a ^{32}P-labeled *VEGF/VPF* cDNA probe synthesized by PCR with the forward and reverse oligonucleotide primers. The hybridized filters were autoradiographed using Kodak® XAR film at −80°C for 16–18 h or exposed to a storage phosphor screen (Molecular Dynamics/GE Healthcare Bio-Sciences, Pittsburgh, PA) for 5 h. The radioactivity, which was proportional to the amount of *VEGF/VPF* mRNA, was quantified using a PhosphorImager (model no. 410A; Molecular Dynamics/GE Healthcare Bio-Sciences) and was normalized by the amount of rRNA.

Statistical Analysis

Statistical analyses were performed using SPSS® version 21 (IBM Corp., Chicago, IL). Data presented are expressed as mean ± SEM. We used Wilcoxon signed-rank tests to compare vascular permeability and mast cell degranulation levels among groups.

RESULTS

Radiation-Induced Dose-Dependent Increase in Vascular Permeability

Using C3H mouse dorsal skin chambers and intravital microscopy, we determined the kinetics of dermal vascular permeability before, and at 1, 5 and 24 h, and 3, 5 and 10 days after 15 and 50 Gy irradiation (Table 1). Statistically significant increases in vascular permeability were observed as early as 5 h after 50 Gy irradiation and by 24 h after 15 Gy irradiation ($P < 0.05$).

For all three radiation doses tested, 2, 15 and 50 Gy, vascular permeability peaked at 24 h after irradiation, with increases of 1.5-, 2.4- and 6.4-fold from the baseline, respectively (Fig. 2). The permeability gradually receded to the baseline level by day 3, 5 and 10 after 2, 15 and 50 Gy irradiation, respectively (Fig. 2). These results indicate that the extent and duration of the increase in vascular permeability are dependent on the radiation dose.

TABLE 1
Vascular Permeability Coefficients in the C3H Mouse Dorsal Skin Chamber after Irradiation

Time after irradiation	15 Gy (n)	50 Gy (n)
Baseline	5.3 ± 0.5 (11)	7.6 ± 1.3 (5)
1 h	5.6 ± 0.4 (3)	14.0 ± 5.9 (3)
5 h	2.6 ± 1.2 (3)	20.8 ± 2.5* (3)
1 day	12.8 ± 1.3* (5)	47.2 ± 12.4* (3)
3 days	9.3 ± 1.6*(6)	20.4 ± 2.0* (3)
5 days	5.0 ± 0.9 (6)	18.6 ± 3.9* (4)
10 days	5.1 ± 2.6 (3)	5.6 ± 3.1 (3)

Notes. Data are expressed as mean ± SEM; n = number of mice. *$P < 0.05$ compared with the corresponding baseline level.

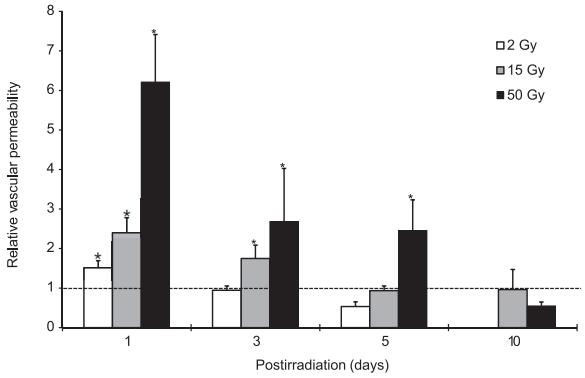

FIG. 2. Alteration of vascular permeability in the skin after irradiation. Relative changes in vascular permeability from the baseline levels in the C3H mouse dorsal skin chamber are shown (see Table 1 for the actual permeability coefficient data). One day after irradiation with 2, 15 and 50 Gy, the vascular permeability increased by 1.5, 2.4 and 6.2 times, respectively, and then gradually decreased to baseline levels by day 3, 5 and 10, respectively (*$P < 0.05$).

Radiation-Induced Mast Cell Degranulation

After irradiation, skin mast cell degranulation was determined by Giemsa staining (Fig. 3). Individual mast cells were scored as normal (Fig. 3A), moderately degranulated (Fig. 3B) or extensively degranulated (Fig. 3C). There were some degranulated mast cells observed in the control tissue, and the fraction of moderately degranulated mast cells was not significantly affected by radiation; however, the fraction of extensively degranulated mast cells significantly increased at 24 h after 15 Gy irradiation ($P < 0.05$; Fig. 3D). We also confirmed mast cell degranulation by electron microscopy. ''Normal'' mast cells maintained dense, intact granules in the cytoplasm (Fig. 3E). On the other hand, there were many empty vacuoles and some granules with decreased density in the degranulated mast cells observed at 24 h after irradiation (Fig. 3F).

Radiation Did Not Affect VEGF and NOS

No appreciable changes were observed in the protein levels of VEGF and eNOS in the C3H mouse skin before and at day 0–5 after 15 Gy irradiation. There were also no changes in the mRNA transcript levels of *VEGF* (Fig. 4). We could not detect iNOS in any sample, regardless of treatment and time.

Radiation Did Not Affect Vascular Permeability in Mast Cell-Deficient Mice

To examine the contribution of mast cells to radiation-induced hyperpermeability, we compared the vascular permeability in mast cell-deficient WW^v versus wild-type mice. There was no increase in vascular permeability from the baseline at 24 h after 15 Gy irradiation in WW^v mice (Fig. 5). On the other hand, the same radiation dose significantly increased vascular permeability in the wild-type mice.

DISCUSSION

Radiation and Vascular Permeability

Using a transparent window model and intravital microscopy, we successfully monitored vascular permeability in the mouse skin for up to 10 days after a single dose of local radiation. There was a strong positive correlation between both the extent and duration of vascular hyperpermeability and radiation dose ranging from 2 to 50 Gy. This result is in good agreement with a previous published report by Krishnan *et al*., demonstrating dose-dependent effects of single doses of 2–30 Gy of radiation (applied with a 15 MV X ray) on extravasation of radiolabeled albumin in the hind limb skeletal muscle of New Zealand white rabbits (*41*).

The onset of vascular permeability elevation is also radiation dose-dependent and may depend on tissue type as well. Macromolecular leakage in the skin or intestine was reported to increase as early as minutes or hours after irradiation (*1, 5, 7, 41, 42*). In our study, there was some increase in permeability observed at 1 h after 50 Gy irradiation, and the increase was statistically significant at 5 h. In the lower dose groups (2 and 15 Gy), the increase in vascular permeability became significant only at 24 h after irradiation. Regardless of the radiation dose, we observed a peak in the increase of vascular permeability at 24 h after irradiation. Similarly, Song *et al*. reported peak extravasation of plasma protein at 18 h after irradiation in the epidermis and dermis of guinea pigs (*1*). Similar increases in vascular permeability at 18–24 h after irradiation have been observed in different organs (*2, 6*).

The duration of the vascular hyperpermeability after irradiation was also dose dependent in our study. The increased permeability gradually decreased back to the baseline level by day 3, 5 and 10 after 2, 15 and 50 Gy irradiation, respectively. Krishnan *et al*. reported that normal vascular function was restored within 24 h at lower radiation doses (up to 6 Gy). The radiolabeled albumin leakage returned to the baseline level by day 10 after 15 Gy irradiation and remained high for up to 30 days after 20 Gy irradiation.

Several published studies have shown a biphasic increase in vascular permeability (*2, 4*). Law *et al*. found that 20 Gy

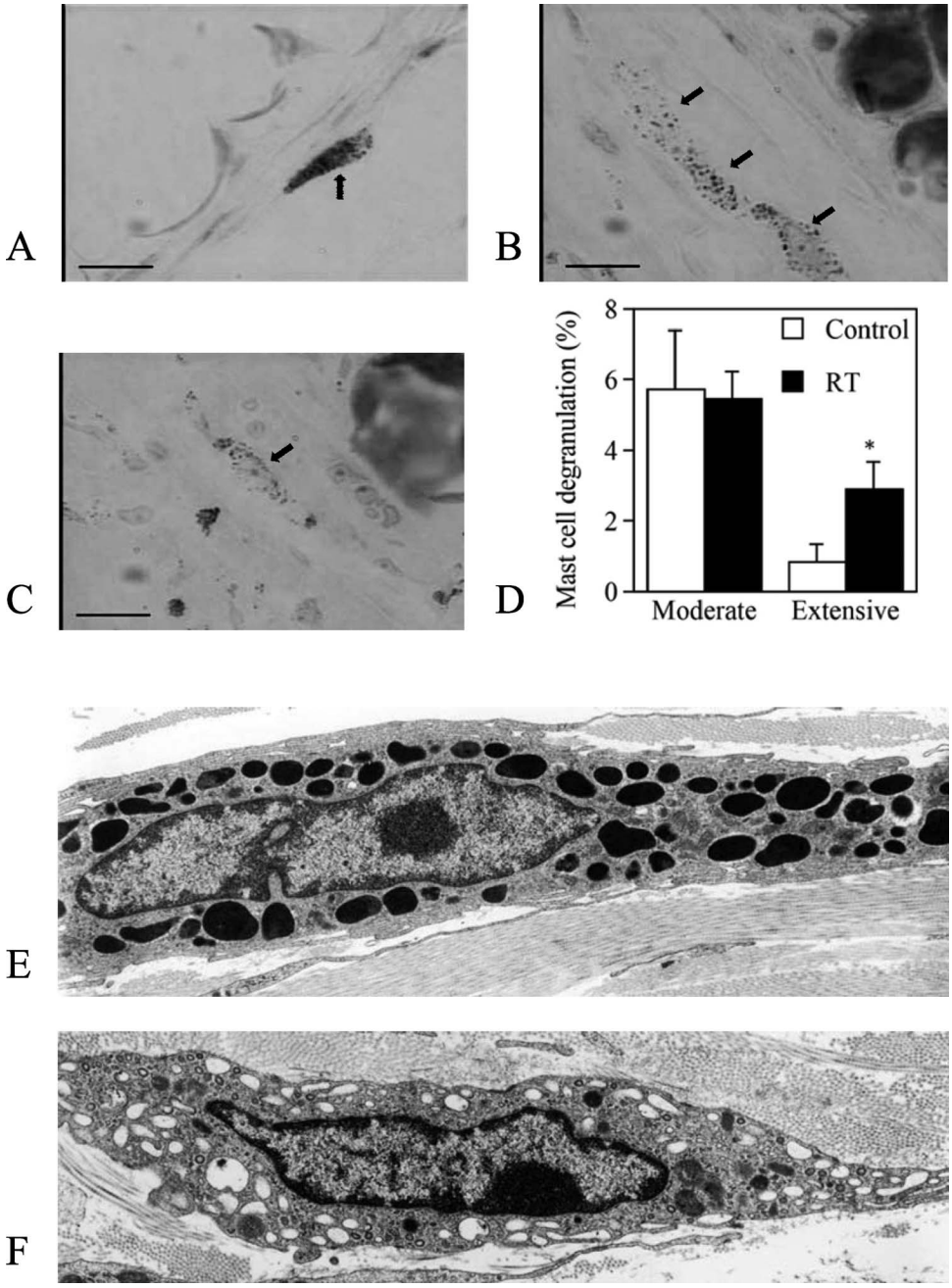

FIG. 3. Normal mast cells in control C3H mice (panel A) and moderately (panel B) and extensively (panel C) degranulated mast cells (arrows) in the ear skin of C3H mice at 24 h after 15 Gy irradiation (bar, 20 μm; 630× original magnification). Panel D: Quantification of mast cell degranulation based on Giemsa staining. Fractions of moderately and extensively degranulated mast cells are shown. n = 3 per group; $*P < 0.05$ vs. nonirradiated control. Panels E and F: Electron microscopy (3,000×) of a normal mast cell with its granules (panel E) and a degranulated mast cell with some empty vacuoles and granules with decreased density (panel F).

irradiation of the rat ear increased albumin extravasation at day 1 after irradiation and then again at 3–4 weeks after irradiation (*2*). The lung permeability surface area to albumin after 18 Gy irradiation to the entire thorax of Sprague Dawley rats showed a biphasic increase: the permeability surface area increased immediately after irradiation, remained elevated for 3 days, fell back to normal levels and then increased again markedly at day 18 after irradiation (*4*). We did not observe late-phase hyperpermeability within up to 10 days of our observation period.

Mechanism of Radiation-Induced Vascular Hyperpermeability

The relationship of mast cell degranulation to the increase of vascular permeability observed after radiation exposure was first proposed in the 1950s (*24, 26, 28*), although the

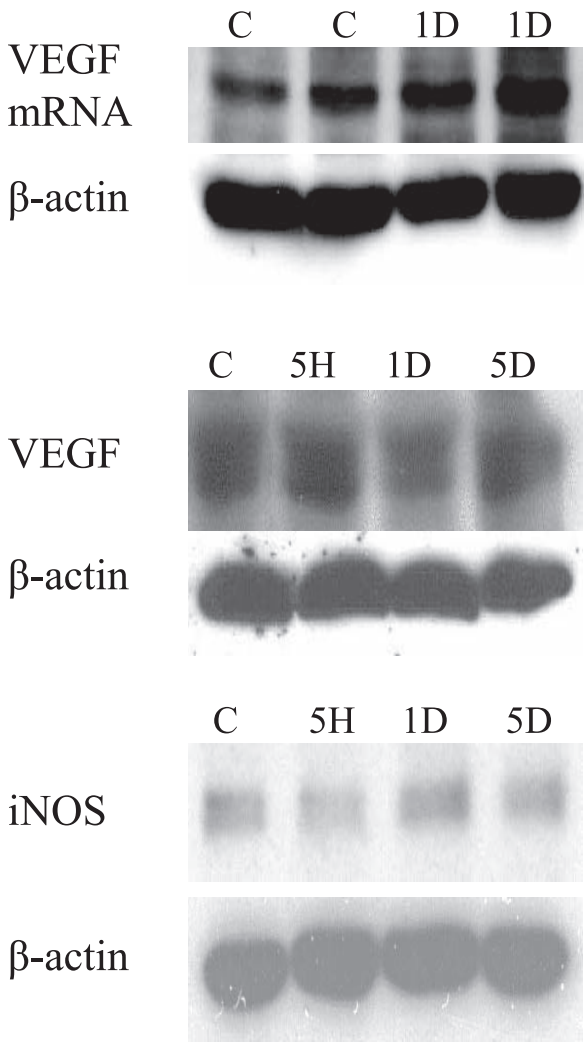

FIG. 4. Northern (top panel) and Western (middle panel) blot analysis of vascular endothelial growth factor (VEGF) and Western blot analysis (bottom panel) of endothelial nitric oxide synthase (eNOS) in the skin of C3H mice. Overall, the tissue mRNA and protein VEGF levels and eNOS protein levels in the C3H mouse skin did not change after 15 Gy irradiation.

mechanism underlying this effect remains somewhat elusive.

Given this background, we designed the current study to directly test the role of mast cells in radiation-induced hyperpermeability, and found a relationship between mast cell degranulation and vascular hyperpermeability after irradiation. In particular, the number of extensively degranulated mast cells significantly increased at 24 h after 15 Gy irradiation to the skin of mice, and this increase coincided with an increase in vascular permeability. However, no increase in vascular permeability was observed in the mast cell-deficient mice. These results strongly suggest that histamine released by mast cell degranulation plays an important role in the early increase of vascular permeability after irradiation.

Mast cells are known to produce and secrete VEGF (*22*). However, we did not detect appreciable changes in the

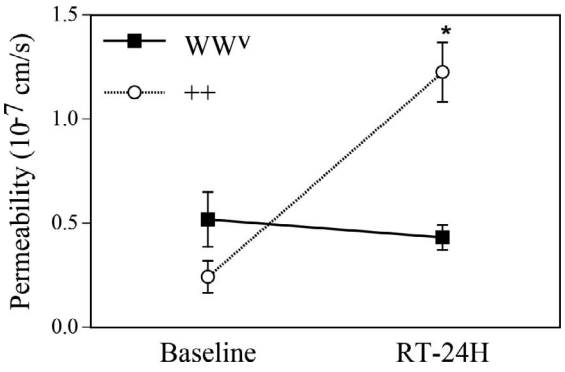

FIG. 5. Effect of mast cell depletion on radiation-induced vascular hyperpermeability. Vascular permeability coefficients in mast cell-deficient (WW^v) mice (n = 3) and their wild-type (++) littermates (n = 3) before and 24 h after 15 Gy irradiation. *$P < 0.05$ compared to corresponding wild-type mice.

overall tissue mRNA or protein level of VEGF after irradiation to the skin in either WW^v or wild-type mice. This might reflect the fact that radiation-induced changes in VEGF levels occur only in mast cells from a relatively small fraction of the irradiated skin. However, in previous work, VEGF was found to be upregulated in the central nervous system tissue at 8–20 weeks after 22 Gy irradiation (*33*), and anti-VEGF antibody therapy could mitigate the development of radiation-induced necrosis in the mouse brain at 4–13 weeks after irradiation (*43*). Therefore, VEGF may be involved in the relatively late phase of radiation-induced injury.

Similarly, the involvement of NO in radiation-induced injuries may depend on the tissue type and time point considered. Radiation-induced iNOS mRNA expression in the ileum but not the colon within 2 h (*44*) and also induced iNOS expression in lung alveolar macrophages (*45*). However, NOS activity in the spinal cord did not change after irradiation (*46*). In our study, iNOS was not detected in the irradiated skin of mice and the eNOS protein level did not change after irradiation. Since eNOS is constitutively expressed in vascular endothelial cells and NO production from eNOS is regulated by the intracellular calcium level, the NO production rate could change after radiation exposure without inducing a change in the overall eNOS protein level.

Collectively, using a novel method to measure vascular permeability, our results demonstrate that radiation induces vascular hyperpermeability in a dose-dependent manner and that mast cells mediate this increase. Further studies are needed to determine the molecular mechanism of radiation-induced mast cell degranulation to develop novel strategies for protecting normal tissue from radiation-induced injury.

ACKNOWLEDGMENTS

We thank Dr. Stephen J. Galli for his helpful advice, Dr. Kathy Held for her help with the irradiation of mice, Ms. Julia Kahn for her help with small animal surgery and Dr. Young Kun Deung for his help with the electron microscopy experiments. This research was supported in part by

the National Institutes of Health [grant nos. R35-CA056591 (RKJ), P01-CA080124 (RKJ and DF) and R01-CA096915 (DF)]. No competing interests exist.

Received: July 1, 2015; accepted: December 9, 2015; published online: January 15, 2016

REFERENCES

1. Song CW, Anderson RS, Tabachnick J. Early effects of beta irradiation on dermal vascular permeability to plasma proteins. Radiat Res 1966; 27:604–15.
2. Law MP, Thomlinson RH. Vascular permeability in the ears of rats after x-irradiation. Br J Radiol 1978; 51:895–904.
3. Law MP. Vascular permeability and late radiation fibrosis in mouse lung. Radiat Res 1985; 103:60–76.
4. Evans ML, Graham MM, Mahler PA, Rasey JS. Changes in vascular permeability following thorax irradiation in the rat. Radiat Res 1986; 107:262–71.
5. Krishnan L, Krishnan EC, Jewell WR. Immediate effect of irradiation on microvasculature. Int J Radiat Oncol Biol Phys 1988; 15:147–50.
6. Gaber MW, Yuan H, Killmar JT, Naimark MD, Kiani MF, Merchant TE. An intravital microscopy study of radiation-induced changes in permeability and leukocyte-endothelial cell interactions in the microvessels of the rat pia mater and cremaster muscle. Brain Res Brain Res Protoc 2004; 13:1–10.
7. Gabrys D, Greco O, Patel G, Prise KM, Tozer GM, Kanthou C. Radiation effects on the cytoskeleton of endothelial cells and endothelial monolayer permeability. Int J Radiat Oncol Biol Phys 2007; 69:1553–62.
8. Jolles B, Harrison RG. Enzymic processes in vascular permeability and fragility changes in the skin radiation reaction. Bibl Anat 1967; 9:482–7.
9. Jolles B, Harrison RG. Enzymic processes and vascular changes in the skin radiation reaction. Br J Radiol 1966; 39:12–8.
10. Mount D, Bruce WR. Local plasma volume and vascular permeability of rabbit skin after irradiation. Radiat Res 1964; 23:430–45.
11. Studer R, Potchen J. The radioisotopic assessment of regional microvascular permeability to macromolecules. Microvasc Res 1971; 3:35–48.
12. Baumgarten A, Melrose GJ, Vagg WJ. Continuous quantitative recording of changes in vascular permeability. Experientia 1967; 23:884–5.
13. Loyd JE, Bolds JM, Sheller JR, Duke SS, Gillette AW, Malcolm AW, et al. Acute effects of thoracic irradiation on lung function and structure in awake sheep. J Appl Physiol (1985) 1987; 62:208–18.
14. Graham MM, Evans ML. A simple, dual tracer method for the measurement of transvascular flux of albumin into the lung. Microvasc Res 1991; 42:266–79.
15. Siegal T, Pfeffer MR. Radiation-induced changes in the profile of spinal cord serotonin, prostaglandin synthesis, and vascular permeability. Int J Radiat Oncol Biol Phys 1995; 31:57–64.
16. Graham MM, Evans ML. The measurement of capillary permeability changes in the irradiated rat using a double isotope technique. AFRRI Scientific Report 71-12. Bethesda: Armed Forces Radiobiology Research Institute; 1971.
17. Moding EJ, Clark DP, Qi Y, Li Y, Ma Y, Ghaghada K, et al. Dual-energy micro-computed tomography imaging of radiation-induced vascular changes in primary mouse sarcomas. Int J Radiat Oncol Biol Phys 2013; 85:1353–9.
18. Yuan F, Leunig M, Berk DA, Jain RK. Microvascular permeability of albumin, vascular surface area, and vascular volume measured in human adenocarcinoma LS174T using dorsal chamber in SCID mice. Microvasc Res 1993; 45:269–89.
19. Leunig M, Yuan F, Menger MD, Boucher Y, Goetz AE, Messmer K, et al. Angiogenesis, microvascular architecture, microhemodynamics, and interstitial fluid pressure during early growth of human adenocarcinoma LS174T in SCID mice. Cancer Res 1992; 52:6553–60.
20. Monsky WL, Fukumura D, Gohongi T, Ancukiewcz M, Weich HA, Torchilin VP, et al. Augmentation of transvascular transport of macromolecules and nanoparticles in tumors using vascular endothelial growth factor. Cancer Res 1999; 59:4129–35.
21. Donlon MA. Role of mast cell mediators in radiation injury and protection. Pharmacol Ther 1988; 39:373–7.
22. Boesiger J, Tsai M, Maurer M, Yamaguchi M, Brown LF, Claffey KP, et al. Mast cells can secrete vascular permeability factor/vascular endothelial cell growth factor and exhibit enhanced release after immunoglobulin E-dependent upregulation of fc epsilon receptor I expression. J Exp Med 1998; 188:1135–45.
23. Nagy JA, Benjamin L, Zeng H, Dvorak AM, Dvorak HF. Vascular permeability, vascular hyperpermeability and angiogenesis. Angiogenesis 2008; 11:109–19.
24. Lasser EC, Stenstrom KW. Elevation of circulating blood histamine in patients undergoing deep roentgen therapy. Am J Roentgenol Radium Ther Nucl Med 1954; 72:985–8.
25. Salazar OM, Rubin P, Keller B, Scarantino C. Systemic (half-body) radiation therapy: response and toxicity. Int J Radiat Oncol Biol Phys 1978; 4:937–50.
26. Van Den Brenk HA. Observations on mast cell changes, histamine release and local tissue damage in rats following x-irradiation. Br J Exp Pathol 1958; 39:356–66.
27. Kitamura Y, Yokoyama M, Sonoda T, Mori KJ. Different radiosensitivities of mast-cell precursors in the bone marrow and skin of mice. Radiat Res 1983; 93:147–56.
28. Conte FP, Melville GS, Jr., Upton AC. Effects of graded doses of wholebody x-irradiation on mast cells in the rat mesentery. Am J Physiol 1956; 187:160–2.
29. Willoughby DA. Pharmacological aspects of the vascular permeability changes in the rat's intestine following abdominal radiation. Br J Radiol 1960; 33:515–9.
30. Albrecht M, Muller K, Kohn FM, Meineke V, Mayerhofer A. Ionizing radiation induces degranulation of human mast cells and release of tryptase. Int J Radiat Biol 2007; 83:535–41.
31. Graham MM, Evans ML, Dahlen DD, Mahler PA, Rasey JS. Pharmacological alteration of the lung vascular response to radiation. Int J Radiat Oncol Biol Phys 1990; 19:329–39.
32. Carmeliet P, Jain RK. Angiogenesis in cancer and other diseases. Nature 2000; 407:249–57.
33. Tsao MN, Li YQ, Lu G, Xu Y, Wong CS. Upregulation of vascular endothelial growth factor is associated with radiation-induced blood-spinal cord barrier breakdown. J Neuropathol Exp Neurol 1999; 58:1051–60.
34. Fukumura D, Yuan F, Endo M, Jain RK. Role of nitric oxide in tumor microcirculation. Blood flow, vascular permeability, and leukocyte-endothelial interactions. Am J Pathol 1997; 150:713–25.
35. Fukumura D, Gohongi T, Kadambi A, Izumi Y, Ang J, Yun CO, et al. Predominant role of endothelial nitric oxide synthase in vascular endothelial growth factor-induced angiogenesis and vascular permeability. Proc Natl Acad Sci U S A 2001; 98:2604–9.
36. Yuan F, Salehi HA, Boucher Y, Vasthare US, Tuma RF, Jain RK. Vascular permeability and microcirculation of gliomas and mammary carcinomas transplanted in rat and mouse cranial windows. Cancer Res 1994; 54:4564–8.
37. Dvorak HF, Mihm MC, Jr, Dvorak AM, Barnes BA, Manseau EJ, Galli SJ. Rejection of first-set skin allografts in man. the microvasculature is the critical target of the immune response. J Exp Med 1979; 150:322–37.
38. Galli SJ, Hammel I. Unequivocal delayed hypersensitivity in mast cell-deficient and beige mice. Science 1984; 226:710–3.

39. Martin TR, Galli SJ, Katona IM, Drazen JM. Role of mast cells in anaphylaxis. Evidence for the importance of mast cells in the cardiopulmonary alterations and death induced by anti-IgE in mice. J Clin Invest 1989; 83:1375–83.

40. Wershil BK, Murakami T, Galli SJ. Mast cell-dependent amplification of an immunologically nonspecific inflammatory response. Mast cells are required for the full expression of cutaneous acute inflammation induced by phorbol 12-myristate 13- acetate. J Immunol 1988; 140:2356–60.

41. Krishnan EC, Krishnan L, Jewell B, Bhatia P, Jewell WR. Dose-dependent radiation effect on microvasculature and repair. J Natl Cancer Inst 1987; 79:1321–5.

42. Panes J, Anderson DC, Miyasaka M, Granger DN. Role of leukocyte-endothelial cell adhesion in radiation-induced microvascular dysfunction in rats. Gastroenterology 1995; 108:1761–9.

43. Jiang X, Engelbach JA, Yuan L, Cates J, Gao F, Drzymala RE, et al. Anti-VEGF antibodies mitigate the development of radiation necrosis in mouse brain. Clin Cancer Res 2014; 20:2695–702.

44. MacNaughton WK, Aurora AR, Bhamra J, Sharkey KA, Miller MJ. Expression, activity and cellular localization of inducible nitric oxide synthase in rat ileum and colon post-irradiation. Int J Radiat Biol 1998; 74:255–64.

45. Nozaki Y, Hasegawa Y, Takeuchi A, Fan ZH, Isobe KI, Nakashima I, et al. Nitric oxide as an inflammatory mediator of radiation pneumonitis in rats. Am J Physiol 1997; 272:L651–8.

46. Siegal T, Pfeffer MR, Meltzer A, Shezen E, Nimrod A, Ezov N, et al. Cellular and secretory mechanisms related to delayed radiation-induced microvessel dysfunction in the spinal cord of rats. Int J Radiat Oncol Biol Phys 1996; 36:649–59.